Published in final edited form as:
Magn Reson Med. 2014 December ; 72(6): 1530–1540. doi:10.1002/mrm.25055.

Whole brain 3D T2-weighted BOLD fMRI at 7T

Jun Hua[1,2], **Qin Qin**[1,2], **Peter C. M. van Zijl**[1,2], **James J. Pekar**[1,2], and **Craig K. Jones**[1,2]

[1]The Russell H. Morgan Department of Radiology and Radiological Science, Division of MR Research, The Johns Hopkins University School of Medicine, Baltimore, MD USA

[2]F.M. Kirby Research Center for Functional Brain Imaging, Kennedy Krieger Institute, Baltimore, MD USA

Abstract

Purpose—A new acquisition scheme for T2-weighted spin-echo BOLD fMRI is introduced.

Methods—It employs a T2-preparation module to induce BOLD contrast, followed by a single-shot 3D fast gradient-echo readout with short TE. It differs from most spin-echo BOLD sequences in that BOLD contrast is generated before the readout, which eliminates the "dead time" due to long TE required for T2 contrast, and substantially improves acquisition efficiency. This approach, termed "3D T2prep-GRE", was implemented at 7T with a typical spatial ($2.5\times2.5\times2.5mm^3$) and temporal (TR=2.3s) resolution for fMRI and whole-brain coverage (55 slices), and compared with the widely used 2D spin-echo EPI sequence.

Results—In fMRI experiments of simultaneous visual/motor activities, 3D T2prep-GRE showed minimal distortion and little signal dropout across the whole brain. Its lower power deposition allowed greater spatial coverage (55 versus 17 slices with identical TR, resolution and power level), temporal SNR (60% higher) and CNR (35% higher) efficiency than 2D spin-echo EPI. It also showed smaller T2* contamination.

Conclusion—This approach is expected to be useful for ultra-high field fMRI, especially for regions near air cavities. The concept of using T2-preparation to generate BOLD contrast can be combined with many other sequences at any field strength.

Keywords

blood-oxygenation-level-dependent; T2 preparation; fast gradient echo; turbo field echo; GRE; TFE; high field; SE BOLD

Introduction

High field (7T) human MRI scanners have become available in recent years with the promise of an approximately linear increase in signal-to-noise ratio (SNR) with field strength. In addition, high field is particularly attractive to blood-oxygenation-level-

Corresponding Author: Jun Hua, Johns Hopkins University School of Medicine, Department of Radiology;, Kennedy Krieger Institute, F.M. Kirby Research Center for Functional Brain Imaging, 707 N Broadway, Baltimore, MD, 21205, jhua@mri.jhu.edu, Tel: 443-923-9551, Fax: 443-923-9505.

dependent (BOLD) functional MRI (fMRI) as the BOLD contrast shows a supra-linear increase with field strength (1-6). To date, the majority of BOLD fMRI experiments are performed using gradient echo (GRE) echoplanar-imaging (EPI) sequences. While they provide excellent sensitivity to signal changes during functional stimulation with high acquisition efficiency, they often suffer from geometric distortions and signal dropouts in regions near air cavities such as the orbitofrontal cortex and temporal lobes, which are exacerbated at high field. Spin echo (SE) based sequences are useful alternative approaches to alleviate these problems (5,7,8). More importantly, the T2-weighted contrast in SE BOLD is more specific to the site of neuronal activity at high field than the T2*-weighted contrast in GRE BOLD (2,3,5,9-17), making it an appealing option for brain mapping at high field (8,18). SE BOLD fMRI can be performed using approaches such as fast spin echo (FSE) (19-21), gradient spin echo (GRASE) (22-26), stimulated echoes (27), balanced (28-30) and non-balanced (31,32) steady state free precession (SSFP), RASER (33,34), and most commonly, SE EPI (2,7,8,10,11,13,18,35-37). One of the main constraints for SE sequences, however, is the high power deposition imposed mainly by the large number of refocusing radiofrequency (RF) pulses, which unfortunately scales with the square of the field strength.

The T2 or T2* contrast in most BOLD fMRI methods is generated during the imaging sequence, which may impose some intrinsic constraints. For instance, a long echo time (TE) is required for SE BOLD, which produces some “dead time” that limits the acquisition efficiency and temporal resolution for fMRI. Alternatively, T2 contrast can be induced with driven equilibrium (DE, also known as driven equilibrium Fourier transform or DEFT) (38). In MRI, driven equilibrium was originally used to enhance SNR for SE sequences with short repetition time (TR) (39,40). It was also applied in GRE sequences as a preparation module immediately before the readout train, referred to as T2 preparation or T2-prep (41,42). Early examples of applying this concept include methods that combine T2 preparation with a segmented 3D fast GRE readout for T2-weighted anatomical imaging in the brain (43) and liver (44). Such T2-prepared segmented 3D fast GRE sequences have also been used to improve the contrast between blood and tissue in cardiac imaging (45) and peripheral angiography (46), to detect myocardial perfusion changes (47), in dynamic susceptibility contrast (DSC) cardiac MRI (48), and for myelin water quantification (49). T2 preparation can also be combined with other imaging sequences. For fMRI in the brain, a 3D T2prep-EPI sequence (50) was proposed to combine T2 preparation with a 3D EPI readout for mixed T2- and T2*-weighted BOLD fMRI.

In this study, we propose a new acquisition scheme for T2-weighted BOLD fMRI. The T2 contrast is created using a T2 preparation module, followed immediately by a single-shot 3D fast GRE (also known as turbo field echo, TFE, or TurboFLASH) readout sequence with short TE_{GRE} (<2ms). Such a readout has much less geometric distortion and fewer signal dropouts than EPI as well as low power deposition, and is commonly used in high-resolution anatomical scans such as the Magnetization Prepared RApid Gradient Echo (MPRAGE) sequence (51). Using this 3D T2prep-GRE approach, whole brain fMRI images with minimal distortion and dropouts could be acquired with a spatial resolution of 2.5mm isotropic (55 slices) at a temporal resolution of 2.3s at 7T. Human fMRI experiments with simultaneous flashing checkerboard and bilateral finger tapping were performed to evaluate

the 3D T2prep-GRE approach and compare it with the conventional 2D multi-slice SE EPI sequence. Part of this work has been report in abstract form (52).

Methods

Five healthy human subjects, who gave written informed consent before participating in this Johns Hopkins Institutional Review Board (IRB) approved, Health Insurance Portability and Accountability Act (HIPAA)-compliant study, were scanned on a 7T Philips MRI scanner (Philips Healthcare, Best, The Netherlands). A 32-channel phased-array head coil (Nova Medical, Wilmington, MA, USA) was used for RF reception and a head-only quadrature coil for transmit. Two rectangular pads (23×10×2mm) filled with high dielectric constant materials (53) were placed between the lateral sides of the subjects' head and the coil, in order to improve field homogeneity (54). fMRI sessions were performed using visual stimulation with blue/yellow flashing checkerboard (36.8s off/27.6s on, 4 repetitions, 1 extra off period in the end) delivered using a projector from the back of magnet. The subjects were instructed to perform bilateral finger tapping during the flashing periods. Each fMRI run took 4 minutes and 54.4 seconds during which 128 image volumes (TR=2.3s) were acquired.

Three pseudo-randomized fMRI scans were performed on each subject: (a) 3D T2prep-GRE (illustrated in Figure 1): 55 slices, single shot 3D fast GRE readout, TR_{GRE} (this is the TR between two echoes during the fast GRE readout)/TE_{GRE}=3.6/1.6ms, flip angle (FA)=4°, readout duration=1916ms, turbo direction=radial (k-space traversed in radial scheme), parallel imaging acceleration (SENSE factor)=3×3(APxFH), partial Fourier fraction=1×1(AP×FH, i.e. no partial Fourier here), low-high (centric) phase encoding. A T2 preparation module (90°x-180°y-180°y-90°-x, duration or effective TE=50ms, spatially non-selective; hyperbolic secant adiabatic pulses were used for 180° pulses, duration=15ms, bandwidth=1050Hz, peak B1=15μT, and >95% inversion at 50% B1) was applied immediately before the readout. The same 90° and 180° RF pulses optimized for 7T in previous work (55,56) were used in T2 preparation. Two 180° pulses were used in T2 preparation to compensate phase variations and to suppress inflow effects (57,58). A spoiler gradient was played at the end of T2 preparation on the first phase encoding axis that has the lowest gradient duty cycle to dephase any residual transverse magnetization. (b) 2D multi-slice SE EPI: 17 slices with interleaved order, no gap between slices, TE=50ms, single-shot multi-slice SE EPI, FA=70° (smaller than the Ernst angle (about 110°) to reduce power), SENSE factor=3, partial Fourier fraction=5/8(AP), fat suppression. A SINC RF pulse (duration=5.38ms, bandwidth=816Hz, peak B1=15μT) was used for refocusing. (c) Same as (a) but without the T2 preparation to test whether there are residual BOLD effects induced by the readout. Common parameters in (a-c): field of view (FOV)=210×210mm^2, voxel size =2.5mm isotropic, TR (TR between two consecutive scans)=2.3s. Note that due to the specific absorption rate (SAR) limit, 2D SE EPI can only accommodate fewer than 1/3 of the slices allowed in 3D T2prep-GRE. To compare image quality in the whole brain, another 2D SE EPI scan (d) was performed *without* functional stimulation: 55 slices, a long TR of 9s, with fat suppression, and other parameters identical to fMRI scan (b). The parameters of the 3D T2prep-GRE and 2D SE EPI sequences are compared in Table 1. To demonstrate the potential to be further accelerated, another 3D T2prep-GRE scan (e) was performed on one

subject with the same functional paradigm: voxel=1.5×1.5×1.6mm^3, 84 slices, TR_{GRE}/TE_{GRE}=3.1/1.4ms, readout duration=1674ms, TR=1860ms, partial Fourier fraction=(5/8)×(5/8)(AP×FH), other parameters same as scan (a). High-resolution anatomical images were acquired using MPRAGE (voxel=1mm isotropic, TR/TE/inversion time (TI)=4.0/1.9/563ms, SENSE factor =2×2). Volume shim over a 120×120×50mm^3 (APxRLxFH) volume centered on the brain was applied in all scans to achieve a reasonably homogeneous field (B0) across the entire brain. As EPI is much more sensitive to susceptibility-induced B0 field inhomogeneity, the SE EPI fMRI scan (b) was also repeated with optimal high order shim in the whole brain (over the same volume as the volume shim), and in the visual cortex only (APxRLxFH=40×120×50mm^3), using the localized shimming tool developed by Schär et al (59). In both cases, a water line width of <60Hz was achieved.

Data analysis was carried out using the Statistical Parametric Mapping (SPM8, University College London, UK) software package and several in-house Matlab R2009b (Mathworks, Natick, MA, USA) routines. Preprocessing steps for fMRI images include realignment to correct for subject motion during the scans, detrending, slice timing correction for 2D multi-slice SE EPI (not needed for 3D scans), co-registration between fMRI and anatomical images, and segmentation to get grey matter (GM) masks. No spatial smoothing was applied in the fMRI analysis. A general linear model was employed to detect functional activation (p-value adjusted with family-wise error<0.05, cluster size≥4). The fractional signal in each voxel was computed by normalizing to the average baseline signal. The relative signal change (ΔS/S) was defined as the difference of fractional signals between resting and activation periods. Temporal SNR (tSNR) was calculated as the signal divided by standard deviation along the time course in each voxel. Contrast-to-noise ratio (CNR) was taken as the product of tSNR and ΔS/S. tSNR and CNR efficiency were defined as tSNR and CNR divided by the square root of acquisition time (in seconds) per slice, respectively, similar to previous studies (49,60).

Results

Figure 2 shows representative images from MPRAGE (anatomical), 3D T2prep-GRE (fMRI scan a) and 2D multi-slice SE EPI (no stimulation, scan d). Geometric distortion is visible in SE EPI images, especially in the frontal and temporal lobes (red arrows). On the other hand, 3D T2prep-GRE images show quite minimal distortion and dropouts across the entire brain. Note that this was achieved with only volume shim to ensure a reasonably homogeneous B0 across the whole brain.

Representative fMRI results from one subject are shown in Figure 3. Robust activation in both visual (mainly row 2) and motor (mainly row 5) cortices was detected with 3D T2prep-GRE (Figure 3a), which is expected from the simultaneous flashing checkerboard and bilateral finger tapping task. Activations in some other cortical regions such as the anterior temporal (row 2) and posterior parietal (row 6) regions were also observed in this subject, which might be related to visual and sensorimotor responses (61,62), or simply the result of large noise in single subject level analysis. The details of these activations are unclear to us and beyond the scope of this methodology study, which certainly warrant further investigation possibly with group level analysis. With the same temporal (TR) and spatial

resolution, 2D SE EPI (Figure 3b) can only cover the visual cortex due to power deposition constraints (SAR). Note that the SE EPI slices here were angled to cover as much cortex as possible and to avoid orbitofrontal cortex, while the SE EPI images shown in Figure 2 were aligned with the Anterior and Posterior commissure (AC-PC) line. Robust activation was detected in the visual cortex with 2D SE EPI. Similar activation patterns in the visual cortex were observed for these two methods (zoomed in and displayed at the bottom of the panels). The average time courses (Figure 3c) over common activated voxels in the visual cortex from the two scans were comparable, and their temporal characteristics were in general consistent with those of SE BOLD responses in the literature. The standard deviations in the time courses are greater than those of ΔS/S in Table 2, as they represent inter-voxel variations in this subject, while the latter reflect inter-subject variations.

Table 2 summarizes the fMRI results from all subjects (n=5). Slightly more activated voxels ($P<0.1$) in the visual cortex were detected with 2D SE EPI. When averaging over voxels activated in both scans, relative signal change (ΔS/S), tSNR, CNR and t-score were all slightly higher ($P<0.1$) in 2D SE EPI, whereas tSNR and CNR efficiency were both significantly greater ($P<0.05$) in 3D T2prep-GRE. Representative tSNR efficiency maps from both methods are shown in Figure 4. No spatial smoothing was performed in the initial analysis to minimize its potential influence for the comparison. To show the effects from spatial smoothing, we also processed the data after applying a Gaussian smoothing kernel with a full-width at half maximum (FWHM) of 5mm. The results remained comparable to those obtained without smoothing, with a slight trend of more activated voxels and smaller ΔS/S in both sequences (not statistically significant, $P>0.1$). A region-of-interest (ROI) based analysis was also performed, in which signals were averaged over the GM voxels in primary visual and motor cortex, respectively. Similar trends in ΔS/S, tSNR, CNR, t-score, and tSNR and CNR efficiency were observed. Volume shim was applied in all these scans to achieve a reasonably homogeneous B0 across the entire brain and compare the two methods under the same B0 shim condition. As EPI is much more sensitive to B0 inhomogeneity than 3D fast GRE, the SE EPI fMRI scan (b) was repeated with optimal high order shim in the visual cortex. The fMRI results in the visual cortex were comparable to those obtained with volume shim (Table 2). Similar results were also obtained with optimal high order shim in the entire brain (data not shown).

The fMRI scans using 3D fast GRE without T2 preparation (Methods, fMRI scan c) yielded a small number of activated voxels in the whole brain (99±64 for visual and motor cortex combined, n=5). The relative signal changes (ΔS/S) in these scans averaged over all activated voxels in the previous 3D T2prep-GRE scans (Methods, fMRI scan a) were not significantly different from baseline for all five subjects ($P>0.1$). A typical time course from one subject is shown in Figure 3c (ΔS/S=0.37±0.57%).

Figure 5 shows fMRI results from one subject using the 3D T2prep-GRE sequence with a voxel size of $1.5\times1.5\times1.6mm^3$, 84 slices and a TR of 1860ms. Similar to fMRI scan (a) with 2.5mm isotropic voxel, minimal distortion was seen in the images and robust activation in visual and motor cortices was detected.

Discussion

A new T2-weighted BOLD fMRI pulse sequence, 3D T2prep-GRE, which consists of a T2 preparation module to create SE BOLD contrast followed by a single-shot 3D fast GRE readout with short TE_{GRE}, is introduced. The "decoupling" of BOLD contrast generation from the readout sequence substantially reduces the "dead time" due to long TE required in SE BOLD and gives more freedom to choose various readout sequences. Compared to the widely used 2D multi-slice SE EPI sequence, the main advantages of the 3D T2prep-GRE approach include: minimal geometric distortion across the whole brain as well as lower SAR, allowing greater spatial coverage and tSNR and CNR efficiency. 3D fast GRE readout with short TE_{GRE} is less sensitive to magnetic susceptibility variations than EPI, and is commonly used in high-resolution anatomical imaging sequences such as MPRAGE. The readout in 3D T2prep-GRE is similar to that in MPRAGE, resulting in fMRI images that resemble anatomical images, which makes spatial alignment easier than for EPI images with nonlinear distortion. One of the major factors that limit spatial coverage in SE EPI is power deposition. This is less of a concern for 3D T2prep-GRE, mainly because only two refocusing 180° pulses are deployed in each TR and small flip angle (4°) RF pulses are used in the readout train. The 3D readout also permits parallel imaging in two phase encoding directions, rather than one in the case of 2D SE EPI, which can be employed to further improve acquisition efficiency. As demonstrated here, 55 slices could be acquired with 3D T2prep-GRE while 2D SE EPI could cover merely 17 slices with the same TR, spatial resolution and SAR level (Table 1). When averaged over commonly activated voxels in the visual cortex, tSNR was 11% lower in 3D T2prep-GRE, mainly due to the small flip angle used in the readout and the high SENSE factor in two directions. However, its tSNR efficiency was 60% higher than 2D SE EPI (Table 2). In ROI based analysis, the tSNR difference between the two methods was minimal, while tSNR efficiency in 3D T2prep-GRE was 92% greater.

2D multi-slice SE EPI is by far the most commonly used sequence for T2-weighted SE BOLD fMRI. A long echo train is often needed, in which only the echo at TE is perfectly refocused. This introduces some additional T2* weighting in the MR signals, which causes geometric distortion and results in a larger relative signal change (ΔS/S) during functional activation than expected with a pure T2-weighted SE BOLD (2,10,13,21,63,64). 3D fast GRE with *long* TE_{GRE} has been employed for T2*-weighted GRE BOLD especially in many early fMRI studies (65-67). Here, in 3D T2prep-GRE, the shortest possible TE_{GRE} (usually <2ms) was used in the GRE readout allowing us to minimize T2* effects. This was demonstrated with fMRI experiments using 3D fast GRE *without* T2 preparation, which had few activated voxels in the brain and relative signal changes (ΔS/S) that were not significantly different from baseline when averaged over activated voxels in fMRI scans with T2 preparation (Figure 3c). The time course and ΔS/S for 3D fast GRE *without* T2 preparation in Figure 3c did show a slight positive trend (albeit not statistically significant) during activation, which implies that there may be still some residual T2* effects induced by the 3D fast GRE readout even with very short TE_{GRE}. Note that this may be an overestimate of T2* effects in the actual T2prep-GRE sequence, as the T2 preparation module will eliminate most intravascular (due to short blood T2 at 7T) and extravascular BOLD effects

around veins, leaving only the extravascular BOLD effects around capillaries due to dynamic averaging to be detected by the following GRE readout. Besides, the underlying mechanisms of the T2* effects in these two sequences are different. In SE EPI, it stems from the echoes acquired at times other than TE that are not perfectly refocused, leading to different T2* effect for each echo, thus varying T2* contamination for different spatial frequency. On the other hand, the T2* effect in 3D fast GRE is the result of free induction decay, which is the same for each echo and independent of spatial frequency, and can be minimized by using shortest TE_{GRE}. Further investigation is warranted to discern these details as how they affect the BOLD contrast in these methods.

The number of activated voxels and ΔS/S (thus CNR and t-score) were all slightly lower in 3D T2prep-GRE than 2D SE EPI, while the CNR efficiency was 35% higher in 3D T2prep-GRE when averaged over commonly activated voxels (Table 2). In ROI based analysis, the differences in ΔS/S, CNR and t-score between the two methods were minimal, while the CNR efficiency was 88% higher in 3D T2prep-GRE (Table 2). The smaller ΔS/S in 3D T2prep-GRE may be attributed to two main factors. First, it may be partially the result of smaller T2* contamination and purer T2-weighted BOLD signals as discussed above. Second, as two refocusing pulses were used in the T2 preparation module (double echo CPMG), the effective T2, thus optimal TE for BOLD contrast, is expected to be longer than a conventional SE EPI sequence with one refocusing pulse. At 7T, the intravascular BOLD effects are negligible due to very short blood T2 values. The extravascular BOLD effects around veins should be largely refocused in SE sequences. Therefore, the dominant contribution to SE BOLD contrast at 7T comes from the extravascular BOLD component around capillaries (dynamic averaging). Based on the theory derived in (4), it is estimated that the equivalent TE to induce the same ΔS/S in a double echo CPMG sequence is approximately 80ms, as compared to 50ms in a single SE sequence. This means that the same TE of 50ms used for both sequences here may lead to a smaller ΔS/S in 3D T2prep-GRE. Thus, using an optimal TE may increase ΔS/S in 3D T2prep-GRE. Note that this potential requirement for longer TE (not TE_{GRE}) in 3D T2prep-GRE will only increase its total TR by 30ms or so. Meanwhile, as physiological noise is dominant in fMRI, the MR signal loss due to a longer TE might only lead to a slight decrease in tSNR (68-71). Further investigation is required to compare single and double SE BOLD contrasts, and to determine the optimal TEs experimentally.

Crusher gradients surrounding the refocusing pulses can be applied in T2 preparation to alleviate problems arising from RF pulse imperfections in T2 preparation caused mainly by B1 field inhomogeneity. On the other hand, it was also suggested (72) that the key to eliminate this problem is to design more robust RF pulses, as crusher gradients can only prevent interference between the residual transverse magnetization and subsequent pulse sequence, but cannot restore the signal loss from inaccurate RF pulse flip angles. In this study, dielectric bags (53,54) were inserted between subjects' head and coil to improve B1 homogeneity, and optimized adiabatic 180° pulses (55,56) that can tolerate a large variation (>50%) in B1 were employed in T2 preparation. However, there still appeared to be some B1 inhomogeneity (hyper-intensity in the middle of the brain in Figure 2). This could be caused mainly by the 90° pulses in T2 preparation and the readout RF pulses. While these artifacts should not undermine the main conclusions in this study, it is important to apply

crusher gradients, design RF pulses with enhanced B1 tolerance and use advanced B1 shimming techniques to improve the accuracy of T2 preparation in future studies. When adding crusher gradients in T2 preparation, it is also important to consider gradient moment nulling (first order) or velocity compensation to suppress motion related artifacts. Here, as the duration of T2 preparation (50ms) is short compared to typical echo train length in sequences such as FSE and GRASE, artifacts due to subject motion are perhaps negligible. Also, considering the very short blood T2 at 7T and long CSF T2, flow related artifacts stemming from T2 preparation are probably minor. In addition, if needed, for instance, when imaging brain regions close to large blood vessels or ventricles, the motion-sensitized driven equilibrium (MSDE) approach (different type of crusher gradients applied in T2 preparation) (56,57,73,74) can be used to minimize confounding signals from fast flowing spins. The MSDE approach can also suppress the inflow effect when very short TRs are used.

Volume shim, which is now widely available on MRI scanners, was used in all scans in order to compare images under the same B0 shim condition. Nevertheless, it should be noted that while 3D T2prep-GRE images are less sensitive to field inhomogeneity, the geometrical distortion in EPI images can be substantially reduced with more advanced B0 shim techniques. We repeated the SE EPI fMRI scans with optimal high order shim in the visual cortex using the localized shimming tool developed by Schär et al (59). The tSNR/CNR results in the visual cortex were similar to those obtained with volume shim (Table 2). This can perhaps be explained by the fact that the occipital lobe was sufficiently well shimmed in both methods with volume shim already, as shown by the image quality in the visual regions in Figures 2, 3 and 5.

The bulk of the power deposition (SAR) in SE sequences comes from the refocusing 180° RF pulses. Therefore, the main reason that 3D T2prep-GRE has lower SAR provided the same 180° pulses are applied is that it only needs two 180° pulses in each volume TR, while the number of 180° pulses in 2D SE EPI is determined by the number of slices and usually far exceeds two. Here, a SINC 180° pulse was used in SE EPI, while a hyperbolic secant adiabatic 180° pulse, which has a higher SAR but a better B1 inhomogeniety tolerance, was employed in T2 preparation (details in Methods). As demonstrated above, the SAR level was still much lower in T2prep-GRE. Besides, the flip angles of the excitation RF pulses in T2prep-GRE are also much smaller than those in SE EPI (4° and 80° here, respectively), which further lowers the SAR. It should be noted that SAR can be reduced by applying RF pulses with longer duration and lower peak B1, and/or variable rate (VR) pulses (also known as variable rate gradient (VRG), or variable rate selective excitation (VERSE) pulses), thus improving spatial coverage for SE sequences (58,75).

Geometic distortion is a well-known problem for EPI that has been studied extensively. Advanced B0 shim techniques can improve global B0 field homogeneity (76,77). A number of approaches have been proposed for local distortion correction in EPI, such as methods based on anatomical images, B0 field maps, point spread function maps, and others (78,79) (and references therein). While these approaches can significantly reduce geometric distortion in EPI, most of them require extra scan time for reference images and sometimes prolonged computational time. Moreover, head motion during fMRI scans may cause non-linear dynamic changes of field susceptibility thus distortion during a fMRI run

(77,78,80,81). Parallel imaging and multiband techniques (35,82-85) can subtantially shorten the echo train in EPI readout, which also mitigates geometric distortion at some expense of SNR. Therefore, a fMRI scan with less intrisic distortion, such as the 3D T2prep-GRE method, may be useful in certain applications.

One confounding factor of the 3D T2prep-GRE sequence is that its signal intensity varies during k-space acquisition mainly due to T1 relaxation. This is inherent to all magnetization prepared 3D fast GRE sequences such as MPRAGE (43,51,86,87), which will lead to spatial blurring/smoothing that deteriorates the spatial resolution and artificially enhances the SNR. Furthermore, for 3D T2prep-GRE, T1 relaxation during the readout echo train will also lower the T2 contrast between baseline and activation for fMRI. As a centric phase encoding profile was used here, the T2-weighted BOLD contrast for higher spatial frequencies may be diminished. The T1 relaxation during readout will also introduce some T1-weighting in T2prep-GRE images, but as T1 change is relatively small during functional activation (88,89) and T1 values become longer and converge (smaller relative difference) at higher fields (90), this effect should have small influence on the BOLD contrast. This confounding issue can be alleviated by using k-space filtering (91) or variable flip angle in the readout echo train (86,87,92). Further investigation is needed to improve this aspect of the T2prep-GRE sequence.

In this study, we focused on the comparison between the proposed 3D T2prep-GRE sequence and 2D SE EPI, currently the most widely used method for T2-weighted SE BOLD fMRI. It should be noted that the 3D GRASE sequence (93,94) is another promising approach and has been gaining popularity for SE BOLD fMRI (22-26). We also tried to implement 3D GRASE on our 7T scanner. With the same TR=2.3s, SAR level<77% (2.5W/kg), slightly shorter TE=40ms due to additional signals from stimulated echoes (22,27) and other parameters identical, 3D GRASE could accommodate 44 slices with the same spatial resolution, slightly less than 3D T2prep-GRE (55 slices). Further investigation is merited for a detailed comparison between these two sequences to characterize their sensitivity (tSNR and CNR), specificity and contrast mechanisms, and to find suitable applications for fMRI.

We chose a voxel size of 2.5mm isotropic in this proof-of-concept study to demonstrate the principle of the 3D T2prep-GRE method for *whole brain coverage*, and to compare it with 2D SE EPI with the same spatial and temporal resolution. The 3D T2prep-GRE method can also be used in fMRI studies focusing on certain regions of the brain, in which case much finer spatial resolution can be obtained with localized coverage (2,11,18,36). In additional, the 3D T2prep-GRE method can be further expedited using techniques such as partial Fourier sampling (95) and multiband. The multiband technique (82,83,85) can substantially speed up many MRI sequences. A recent study (35) demonstrated that using power independent of number of slices (PINS) (84) multiplexing 2D SE EPI at 7T, whole brain coverage can be achieved with 84 slices of 1.6mm thickness, 1.5mm in-plane resolution and a TR of 1860ms using a 4-fold multiband acceleration. With the proposed 3D T2prep-GRE sequence, we were able to achieve *identical* temporal (TR) and spatial (voxel) resolution and coverage using a partial Fourier fraction of 5/8 (typical value for fMRI, other parameters same, centric encoding) *without* multiplexing. Robust activation was detected in the brain with this sequence for a single subject (Figure 5). The main difference here is that in most

SE BOLD approaches such as SE EPI and GRASE, the extent to which their acquisition efficiency can be improved by partial Fourier methods and parallel imaging is limited by the long TE required for T2 contrast, whereas it is no longer a constraint in the readout of 3D T2prep-GRE. One drawback, though, for partial Fourier methods and parallel imaging is that they may have higher SNR penalties than the multiband technique. Nevertheless, the 3D T2prep-GRE sequence may also be further accelerated using the multiband technique in a way similar to 3D multi-slab GRASE (96). Further development is needed to investigate and compare SNR penalties and other characteristics of these sequences.

An important goal for SE BOLD fMRI at ultra-high field is to *simultaneously* achieve sub-mm spatial resolution, whole brain coverage, and TRs of 1-2 seconds or less. This is still not possible with current SE BOLD methods, including the proposed approach. One way to obtain higher spatial resolution is to reduce the field of view. For instance, Heidemann et al. (97) recently introduced a useful method for GRE EPI at 7T. T2prep-GRE can achieve sub-mm resolution with partial brain coverage (less slices, and/or smaller field of view). Several SE EPI BOLD studies in human brain have demonstrated sufficient sensitivity to detect neuronal activity with sub-mm resolution in a single slice (e.g. $0.5\times0.5\times3mm^3$ voxel, TR=6s in (2,11,18); $0.5\times0.5\times1mm^3$ voxel, TR=2s in (36)). As T2prep-GRE is shown to have comparable tSNR/CNR and greater tSNR/CNR efficiency than SE EPI at 2.5mm isotropic voxel size in this study, it is reasonable to expect that T2prep-GRE would also have sufficient sensitivity to detect typical SE BOLD signal changes at sub-mm resolution. Many exciting new technologies are being developed to further improve MRI acquisition efficiency, such as the improvement of multi-channel receiving coils to accelerate parallel imaging as well as the multiband technique (82,83,85). These methods would also greatly benefit T2prep-GRE, and can potentially be combined (96) to further improve its efficiency and sensitivity.

Conclusions

We have demonstrated a new T2-weighted SE BOLD fMRI pulse sequence, 3D T2prep-GRE, which can achieve minimal geometric distortion and signal dropout across the whole brain. Compared to the commonly used 2D multi-slice SE EPI method, it has lower SAR, larger spatial coverage, greater tSNR and CNR efficiency and smaller T2* contamination. This approach is expected to be useful for ultra-high field fMRI scans of the whole brain, or high-resolution scans focusing on specific brain regions, especially those with severe B0 field inhomogeneity. The concept of using T2 preparation to generate BOLD contrast is certainly not limited to EPI (50) and fast GRE, but can be combined with many other fast imaging methods. Although this technique is demonstrated here at 7T, it is readily transferable to any other field strength.

Acknowledgments

The authors thank Mr. Joseph S. Gillen, Ms. Terri Lee Brawner, Ms. Kathleen A. Kahl, and Ms. Ivana Kusevic for experimental assistance. This project was supported by the National Center for Research Resources and the National Institute of Biomedical Imaging and Bioengineering of the National Institutes of Health through resource grant P41 EB015909. Drs. Jun Hua and Craig Jones' salary is paid in part from a grant to the Kennedy Krieger Institute from Philips Healthcare. Equipment used in the study was manufactured by Philips. Dr. van Zijl is a paid lecturer for Philips Medical Systems. Dr. van Zijl is the inventor of technology that is licensed to Philips.

Grant support from NIH-NCRR/NIBIB P41-EB015909.

References

1. Yacoub E, Shmuel A, Pfeuffer J, Van De Moortele PF, Adriany G, Andersen P, Vaughan JT, Merkle H, Ugurbil K, Hu X. Imaging brain function in humans at 7 Tesla. Magn Reson Med. 2001; 45(4):588–594. [PubMed: 11283986]
2. Yacoub E, Duong TQ, Van De Moortele PF, Lindquist M, Adriany G, Kim SG, Ugurbil K, Hu X. Spin-echo fMRI in humans using high spatial resolutions and high magnetic fields. Magn Reson Med. 2003; 49(4):655–664. [PubMed: 12652536]
3. Uludag K, Muller-Bierl B, Ugurbil K. An integrative model for neuronal activity-induced signal changes for gradient and spin echo functional imaging. Neuroimage. 2009; 48(1):150–165. [PubMed: 19481163]
4. Ogawa S, Menon RS, Tank DW, Kim SG, Merkle H, Ellermann JM, Ugurbil K. Functional brain mapping by blood oxygenation level-dependent contrast magnetic resonance imaging. A comparison of signal characteristics with a biophysical model. Biophys J. 1993; 64(3):803. [PubMed: 8386018]
5. Boxerman JL, Hamberg LM, Rosen BR, Weisskoff RM. MR contrast due to intravascular magnetic susceptibility perturbations. Magn Reson Med. 1995; 34(4):555. [PubMed: 8524024]
6. Boxerman JL, Bandettini PA, Kwong KK, Baker JR, Davis TL, Rosen BR, Weisskoff RM. The intravascular contribution to fMRI signal change: Monte Carlo modeling and diffusion-weighted studies in vivo. Magn Reson Med. 1995; 34(1):4–10. [PubMed: 7674897]
7. Bandettini PA, Wong EC, Jesmanowicz A, Hinks RS, Hyde JS. Spin-echo and gradient-echo EPI of human brain activation using BOLD contrast: a comparative study at 1.5 T. NMR Biomed. 1994; 7(1-2):12–20. [PubMed: 8068520]
8. Norris DG. Spin-echo fMRI: The poor relation? Neuroimage. 2012; 62(2):1109–1115. [PubMed: 22245351]
9. Stables LA, Kennan RP, Gore JC. Asymmetric spin-echo imaging of magnetically inhomogeneous systems: theory, experiment, and numerical studies. Magn Reson Med. 1998; 40(3):432–442. [PubMed: 9727947]
10. Duong TQ, Yacoub E, Adriany G, Hu X, Ugurbil K, Kim SG. Microvascular BOLD contribution at 4 and 7 T in the human brain: gradient-echo and spin-echo fMRI with suppression of blood effects. Magn Reson Med. 2003; 49(6):1019–1027. [PubMed: 12768579]
11. Yacoub E, Shmuel A, Logothetis N, Ugurbil K. Robust detection of ocular dominance columns in humans using Hahn Spin Echo BOLD functional MRI at 7 Tesla. Neuroimage. 2007; 37(4):1161–1177. [PubMed: 17702606]
12. Fujita N. Extravascular contribution of blood oxygenation level-dependent signal changes: a numerical analysis based on a vascular network model. Magn Reson Med. 2001; 46(4):723–734. [PubMed: 11590649]
13. Goense JB, Logothetis NK. Laminar specificity in monkey V1 using high-resolution SE-fMRI. Magn Reson Imaging. 2006; 24(4):381–392. [PubMed: 16677944]
14. Harel N, Lin J, Moeller S, Ugurbil K, Yacoub E. Combined imaging-histological study of cortical laminar specificity of fMRI signals. Neuroimage. 2006; 29(3):879–887. [PubMed: 16194614]
15. Zhao F, Wang P, Hendrich K, Ugurbil K, Kim SG. Cortical layer-dependent BOLD and CBV responses measured by spin-echo and gradient-echo fMRI: insights into hemodynamic regulation. Neuroimage. 2006; 30(4):1149. [PubMed: 16414284]
16. Goense JB, Zappe AC, Logothetis NK. High-resolution fMRI of macaque V1. Magn Reson Imaging. 2007; 25(6):740–747. [PubMed: 17499466]
17. Lee SP, Silva AC, Ugurbil K, Kim SG. Diffusion-weighted spin-echo fMRI at 9.4 T: microvascular/tissue contribution to BOLD signal changes. Magn Reson Med. 1999; 42(5):919–928. [PubMed: 10542351]
18. Yacoub E, Harel N, Ugurbil K. High-field fMRI unveils orientation columns in humans. Proc Natl Acad Sci U S A. 2008; 105(30):10607–10612. [PubMed: 18641121]

19. Constable RT, Kennan RP, Puce A, McCarthy G, Gore JC. Functional NMR imaging using fast spin echo at 1.5 T. Magn Reson Med. 1994; 31(6):686–690. [PubMed: 8057823]
20. Gao JH, Xiong J, Li J, Schiff J, Roby J, Lancaster JL, Fox PT. Fast spin-echo characteristics of visual stimulation-induced signal changes in the human brain. J Magn Reson Imaging. 1995; 5(6): 709–714. [PubMed: 8748490]
21. Poser BA, Norris DG. Fast spin echo sequences for BOLD functional MRI. Magma. 2007; 20(1): 11–17. [PubMed: 17245581]
22. De Martino F, Zimmermann J, Muckli L, Ugurbil K, Yacoub E, Goebel R. Cortical Depth Dependent Functional Responses in Humans at 7T: Improved Specificity with 3D GRASE. PLoS One. 2013; 8(3):e60514. [PubMed: 23533682]
23. Feinberg, DA.; Harel, N.; Ramanna, S.; Ugurbil, K.; Yacoub, E. Sub-millimeter Single-Shot 3D GRASE with Inner Volume Selection for T2 weighted fMRI applications at 7 Tesla; Proc 16th Annual Meeting ISMRM; Toronto, Canada. 2008; p. 2373
24. Olman CA, Harel N, Feinberg DA, He S, Zhang P, Ugurbil K, Yacoub E. Layer-specific fMRI reflects different neuronal computations at different depths in human V1. PLoS One. 2012; 7(3):e32536. [PubMed: 22448223]
25. Vu, A.; Feinberg, D.; Harel, N.; Ugurbil, K.; Yacoub, E. Diagonal multi-slab inner volume 3D GRASE imaging for high resolution T2 weighted fMRI; Proc 21st Annual Meeting ISMRM; Salt Lake City, Utah, USA. 2013; p. 2364
26. Zimmermann J, Goebel R, De Martino F, van de Moortele PF, Feinberg D, Adriany G, Chaimow D, Shmuel A, Ugurbil K, Yacoub E. Mapping the organization of axis of motion selective features in human area MT using high-field fMRI. PLoS One. 2011; 6(12):e28716. [PubMed: 22163328]
27. Goerke U, van de Moortele PF. Ugurbil K. Enhanced relative BOLD signal changes in T(2)-weighted stimulated echoes. Magn Reson Med. 2007; 58(4):754–762. [PubMed: 17899596]
28. Dharmakumar R, Qi X, Hong J, Wright GA. Detecting microcirculatory changes in blood oxygen state with steady-state free precession imaging. Magn Reson Med. 2006; 55(6):1372–1380. [PubMed: 16680697]
29. Bieri O, Scheffler K. Effect of diffusion in inhomogeneous magnetic fields on balanced steady-state free precession. NMR Biomed. 2007; 20(1):1–10. [PubMed: 16947639]
30. Miller KL, Jezzard P. Modeling SSFP functional MRI contrast in the brain. Magn Reson Med. 2008; 60(3):661–673. [PubMed: 18727099]
31. Auerbach, EJ.; Heberlein, K.; Hu, X. High-resolution T2 fMRI at high magnetic fields using PSIF; Proc 10th Annual Meeting ISMRM; Honolulu, Hawaii. 2002; p. 2345
32. Barth M, Meyer H, Kannengiesser SA, Polimeni JR, Wald LL, Norris DG. T2-weighted 3D fMRI using S2-SSFP at 7 tesla. Magn Reson Med. 2010; 63(4):1015–1020. [PubMed: 20373402]
33. Chamberlain R, Park JY, Corum C, Yacoub E, Ugurbil K, Jack CR Jr. Garwood M. RASER: a new ultrafast magnetic resonance imaging method. Magn Reson Med. 2007; 58(4):794–799. [PubMed: 17899612]
34. Goerke U, Garwood M, Ugurbil K. Functional magnetic resonance imaging using RASER. Neuroimage. 2011; 54(1):350–360. [PubMed: 20699123]
35. Koopmans PJ, Boyacioglu R, Barth M, Norris DG. Whole brain, high resolution spinecho resting state fMRI using PINS multiplexing at 7 T. Neuroimage. 2012; 62(3):1939–1946. [PubMed: 22683385]
36. Duong TQ, Yacoub E, Adriany G, Hu X, Ugurbil K, Vaughan JT, Merkle H, Kim SG. High-resolution, spin-echo BOLD, and CBF fMRI at 4 and 7 T. Magn Reson Med. 2002; 48(4):589–593. [PubMed: 12353274]
37. De Martino F, Schmitter S, Moerel M, Tian J, Ugurbil K, Formisano E, Yacoub E, de Moortele PF. Spin echo functional MRI in bilateral auditory cortices at 7 T: an application of B(1) shimming. Neuroimage. 2012; 63(3):1313–1320. [PubMed: 22917678]
38. Becker ED, Farrar TC. Driven equilibrium Fourier transform spectroscopy. A new method for nuclear magnetic resonance signal enhancement. J Am Chem Soc. 1969; 91(27):7784–7785. [PubMed: 5357869]
39. van Uijen CM, den Boef JH. Driven-equilibrium radiofrequency pulses in NMR imaging. Magn Reson Med. 1984; 1(4):502–507. [PubMed: 6571572]

40. Maki JH, Johnson GA, Cofer GP, Macfall JR. SNR Improvement in NMR Microscopy Using DEFT. Journal of Magnetic Resonance. 1988; 80(3):482–492.
41. Haase A. Snapshot FLASH MRI. Applications to T1, T2, and chemical-shift imaging. Magn Reson Med. 1990; 13(1):77–89. [PubMed: 2319937]
42. Parrish T, Hu X. A new T2 preparation technique for ultrafast gradient-echo sequence. Magn Reson Med. 1994; 32(5):652–657. [PubMed: 7808267]
43. Mugler JP 3rd, Spraggins TA, Brookeman JR. T2-weighted three-dimensional MP-RAGE MR imaging. J Magn Reson Imaging. 1991; 1(6):731–737. [PubMed: 1823180]
44. Edelman RR, Wallner B, Singer A, Atkinson DJ, Saini S. Segmented turboFLASH: method for breath-hold MR imaging of the liver with flexible contrast. Radiology. 1990; 177(2):515–521. [PubMed: 2171014]
45. Botnar RM, Stuber M, Danias PG, Kissinger KV, Manning WJ. Improved coronary artery definition with T2-weighted, free-breathing, three-dimensional coronary MRA. Circulation. 1999; 99(24):3139–3148. [PubMed: 10377077]
46. Brittain JH, Olcott EW, Szuba A, Gold GE, Wright GA, Irarrazaval P, Nishimura DG. Three-dimensional flow-independent peripheral angiography. Magn Reson Med. 1997; 38(3):343–354. [PubMed: 9339435]
47. Wright KB, Klocke FJ, Deshpande VS, Zheng J, Harris KR, Tang R, Finn JP, Li D. Assessment of regional differences in myocardial blood flow using T2-weighted 3D BOLD imaging. Magn Reson Med. 2001; 46(3):573–578. [PubMed: 11550251]
48. Sakuma H, O'Sullivan M, Lucas J, Wendland MF, Saeed M, Dulce MC, Watson A, Bleyl KL, LaFrance ND, Higgins CB. Effect of magnetic susceptibility contrast medium on myocardial signal intensity with fast gradient-recalled echo and spin-echo MR imaging: initial experience in humans. Radiology. 1994; 190(1):161–166. [PubMed: 8259398]
49. Nguyen TD, Wisnieff C, Cooper MA, Kumar D, Raj A, Spincemaille P, Wang Y, Vartanian T, Gauthier SA. T2 prep three-dimensional spiral imaging with efficient whole brain coverage for myelin water quantification at 1.5 tesla. Magn Reson Med. 2012; 67(3):614–621. [PubMed: 22344579]
50. Denolin V, Metens T. Three-dimensional BOLD fMRI with spin-echo characteristics using T2 magnetization preparation and echo-planar readouts. Magn Reson Med. 2003; 50(1):132–144. [PubMed: 12815688]
51. Mugler JP 3rd, Brookeman JR. Three-dimensional magnetization-prepared rapid gradient-echo imaging (3D MP RAGE). Magn Reson Med. 1990; 15(1):152–157. [PubMed: 2374495]
52. Hua, J.; Jones, CK.; Qin, Q.; van Zijl, PCM. T2-prepared blood-oxygenation-level-dependent (BOLD) fMRI using single-shot 3D fast gradient echo (GRE) sequence with whole brain coverage at 7T; Proc 21st Annual Meeting ISMRM; Salt Lake City, USA. 2013; p. 413
53. Haines K, Smith NB, Webb AG. New high dielectric constant materials for tailoring the B1+ distribution at high magnetic fields. J Magn Reson. 2010; 203(2):323–327. [PubMed: 20122862]
54. Teeuwisse WM, Brink WM, Webb AG. Quantitative assessment of the effects of high-permittivity pads in 7 Tesla MRI of the brain. Magn Reson Med. 2012; 67(5):1285–1293. [PubMed: 21826732]
55. Visser F, Zwanenburg JJ, Hoogduin JM, Luijten PR. High-resolution magnetization-prepared 3D-FLAIR imaging at 7.0 Tesla. Magn Reson Med. 2010; 64(1):194–202. [PubMed: 20572143]
56. Hua J, Jones CK, Qin Q, van Zijl PC. Implementation of vascular-space-occupancy MRI at 7T. Magn Reson Med. 2013; 69(4):1003–1013. [PubMed: 22585570]
57. Wang J, Yarnykh VL, Yuan C. Enhanced image quality in black-blood MRI using the improved motion-sensitized driven-equilibrium (iMSDE) sequence. J Magn Reson Imaging. 2010; 31(5): 1256–1263. [PubMed: 20432365]
58. Conolly S, Glover G, Nishimura D, Macovski A. A reduced power selective adiabatic spin-echo pulse sequence. Magn Reson Med. 1991; 18(1):28–38. [PubMed: 2062239]
59. Schar M, Kozerke S, Fischer SE, Boesiger P. Cardiac SSFP imaging at 3 Tesla. Magn Reson Med. 2004; 51(4):799–806. [PubMed: 15065254]
60. Hu Y, Glover GH. Partial-k-space acquisition method for improved SNR efficiency and temporal resolution in 3D fMRI. Magn Reson Med. 2006; 55(5):1106–1113. [PubMed: 16598724]

61. DeYoe EA, Carman GJ, Bandettini P, Glickman S, Wieser J, Cox R, Miller D, Neitz J. Mapping striate and extrastriate visual areas in human cerebral cortex. Proc Natl Acad Sci U S A. 1996; 93(6):2382–2386. [PubMed: 8637882]
62. Gonzalez-Castillo J, Saad ZS, Handwerker DA, Inati SJ, Brenowitz N, Bandettini PA. Whole-brain, time-locked activation with simple tasks revealed using massive averaging and model-free analysis. Proc Natl Acad Sci U S A. 2012; 109(14):5487–5492. [PubMed: 22431587]
63. Birn, RM.; Bandettini, PA. The effect of T2′ changes on spin-echo EPI derived brain activation maps; Proc 10th Annual Meeting ISMRM; Hawaii, USA. 2002; p. 1324
64. Keilholz, SD.; Silva, AC.; Duyn, JH.; Koretsky, AP. The contribution of T2* to spin-echo EPI: implications for high-field fMRI studies; Proc 13th Annual Meeting ISMRM; Miami, USA. 2005; p. 32
65. Menon RS, Ogawa S, Tank DW, Ugurbil K. 4Tesla gradient recalled echo characteristics of photic stimulation-induced signal changes in the human primary visual cortex. Magn Reson Med. 1993; 30(3):380–386. [PubMed: 8412612]
66. Kim SG, Hendrich K, Hu X, Merkle H, Ugurbil K. Potential pitfalls of functional MRI using conventional gradient-recalled echo techniques. NMR Biomed. 1994; 7(1-2):69–74. [PubMed: 8068528]
67. Haacke EM, Hopkins A, Lai S, Buckley P, Friedman L, Meltzer H, Hedera P, Friedland R, Klein S, Thompson L, et al. 2D and 3D high resolution gradient echo functional imaging of the brain: venous contributions to signal in motor cortex studies. NMR Biomed. 1994; 7(1-2):54–62. [PubMed: 8068526]
68. Gonzalez-Castillo J, Roopchansingh V, Bandettini PA, Bodurka J. Physiological noise effects on the flip angle selection in BOLD fMRI. Neuroimage. 2011; 54(4):2764–2778. [PubMed: 21073963]
69. Kruger G, Kastrup A, Glover GH. Neuroimaging at 1.5 T and 3.0 T: comparison of oxygenation-sensitive magnetic resonance imaging. Magn Reson Med. 2001; 45(4):595–604. [PubMed: 11283987]
70. Kruger G, Glover GH. Physiological noise in oxygenation-sensitive magnetic resonance imaging. Magn Reson Med. 2001; 46(4):631–637. [PubMed: 11590638]
71. Triantafyllou C, Hoge RD, Krueger G, Wiggins CJ, Potthast A, Wiggins GC, Wald LL. Comparison of physiological noise at 1.5 T, 3 T and 7 T and optimization of fMRI acquisition parameters. Neuroimage. 2005; 26(1):243–250. [PubMed: 15862224]
72. Poon CS, Henkelman RM. Practical T2 quantitation for clinical applications. J Magn Reson Imaging. 1992; 2(5):541–553. [PubMed: 1392247]
73. Wang J, Yarnykh VL, Hatsukami T, Chu B, Balu N, Yuan C. Improved suppression of plaque-mimicking artifacts in black-blood carotid atherosclerosis imaging using a multislice motion-sensitized driven-equilibrium (MSDE) turbo spin-echo (TSE) sequence. Magn Reson Med. 2007; 58(5):973–981. [PubMed: 17969103]
74. Balu N, Yarnykh VL, Chu B, Wang J, Hatsukami T, Yuan C. Carotid plaque assessment using fast 3D isotropic resolution black-blood MRI. Magn Reson Med. 2011; 65(3):627–637. [PubMed: 20941742]
75. Conolly S, Nishimura D, Macovski A, Glover G. Variable-rate selective excitation. J Magn Reson. 1988; 78:440–458.
76. Morrell G, Spielman D. Dynamic shimming for multi-slice magnetic resonance imaging. Magn Reson Med. 1997; 38(3):477–483. [PubMed: 9339449]
77. Ward HA, Riederer SJ, Jack CR Jr. Real-time autoshimming for echo planar timecourse imaging. Magn Reson Med. 2002; 48(5):771–780. [PubMed: 12417991]
78. Jezzard P, Clare S. Sources of distortion in functional MRI data. Hum Brain Mapp. 1999; 8(2-3): 80–85. [PubMed: 10524596]
79. Jezzard P. Correction of geometric distortion in fMRI data. Neuroimage. 2012; 62(2):648–651. [PubMed: 21945795]
80. Hutton C, Bork A, Josephs O, Deichmann R, Ashburner J, Turner R. Image distortion correction in fMRI: A quantitative evaluation. Neuroimage. 2002; 16(1):217–240. [PubMed: 11969330]

81. Roopchansingh V, Cox RW, Jesmanowicz A, Ward BD, Hyde JS. Single-shot magnetic field mapping embedded in echo-planar time-course imaging. Magn Reson Med. 2003; 50(4):839–843. [PubMed: 14523971]
82. Feinberg DA, Moeller S, Smith SM, Auerbach E, Ramanna S, Gunther M, Glasser MF, Miller KL, Ugurbil K, Yacoub E. Multiplexed echo planar imaging for sub-second whole brain FMRI and fast diffusion imaging. PLoS One. 2010; 5(12):e15710. [PubMed: 21187930]
83. Moeller S, Yacoub E, Olman CA, Auerbach E, Strupp J, Harel N, Ugurbil K. Multiband multislice GE-EPI at 7 tesla, with 16-fold acceleration using partial parallel imaging with application to high spatial and temporal whole-brain fMRI. Magn Reson Med. 2010; 63(5):1144–1153. [PubMed: 20432285]
84. Norris DG, Koopmans PJ, Boyacioglu R, Barth M. Power Independent of Number of Slices (PINS) radiofrequency pulses for low-power simultaneous multislice excitation. Magn Reson Med. 2011; 66(5):1234–1240. [PubMed: 22009706]
85. Setsompop K, Gagoski BA, Polimeni JR, Witzel T, Wedeen VJ, Wald LL. Blipped-controlled aliasing in parallel imaging for simultaneous multislice echo planar imaging with reduced g-factor penalty. Magn Reson Med. 2012; 67(5):1210–1224. [PubMed: 21858868]
86. Mugler JP 3rd, Epstein FH, Brookeman JR. Shaping the signal response during the approach to steady state in three-dimensional magnetization-prepared rapid gradient-echo imaging using variable flip angles. Magn Reson Med. 1992; 28(2):165–185. [PubMed: 1461121]
87. Epstein FH, Mugler JP 3rd, Brookeman JR. Optimization of parameter values for complex pulse sequences by simulated annealing: application to 3D MP-RAGE imaging of the brain. Magn Reson Med. 1994; 31(2):164–177. [PubMed: 8133752]
88. Lu H, Clingman C, Golay X, van Zijl PC. Determining the longitudinal relaxation time (T1) of blood at 3.0 Tesla. Magn Reson Med. 2004; 52(3):679. [PubMed: 15334591]
89. Grgac K, van Zijl PC, Qin Q. Hematocrit and oxygenation dependence of blood (1) H(2) O T(1) at 7 tesla. Magn Reson Med. 2013; 70(4):1153–1159. [PubMed: 23169066]
90. Rooney WD, Johnson G, Li X, Cohen ER, Kim SG, Ugurbil K, Springer CS Jr. Magnetic field and tissue dependencies of human brain longitudinal 1H2O relaxation in vivo. Magn Reson Med. 2007; 57(2):308–318. [PubMed: 17260370]
91. Deichmann R, Good CD, Josephs O, Ashburner J, Turner R. Optimization of 3-D MP-RAGE sequences for structural brain imaging. Neuroimage. 2000; 12(1):112–127. [PubMed: 10875908]
92. Stocker T, Shah NJ. MP-SAGE: A new MP-RAGE sequence with enhanced SNR and CNR for brain imaging utilizing square-spiral phase encoding and variable flip angles. Magn Reson Med. 2006; 56(4):824–834. [PubMed: 16947341]
93. Feinberg DA, Oshio K. GRASE (gradient- and spin-echo) MR imaging: a new fast clinical imaging technique. Radiology. 1991; 181(2):597–602. [PubMed: 1924811]
94. Oshio K, Feinberg DA. GRASE (Gradient- and spin-echo) imaging: a novel fast MRI technique. Magn Reson Med. 1991; 20(2):344–349. [PubMed: 1775061]
95. Feinberg DA, Hale JD, Watts JC, Kaufman L, Mark A. Halving MR imaging time by conjugation: demonstration at 3.5 kG. Radiology. 1986; 161(2):527–531. [PubMed: 3763926]
96. Chen, L.; Feinberg, D. Simultaneous Multi-Volume GRASE Imaging; Proc 21st Annual Meeting ISMRM; Salt Lake City, Utah, USA. 2013; p. 2365
97. Heidemann RM, Ivanov D, Trampel R, Fasano F, Meyer H, Pfeuffer J, Turner R. Isotropic submillimeter fMRI in the human brain at 7 T: combining reduced field-of-view imaging and partially parallel acquisitions. Magn Reson Med. 2012; 68(5):1506–1516. [PubMed: 22231859]

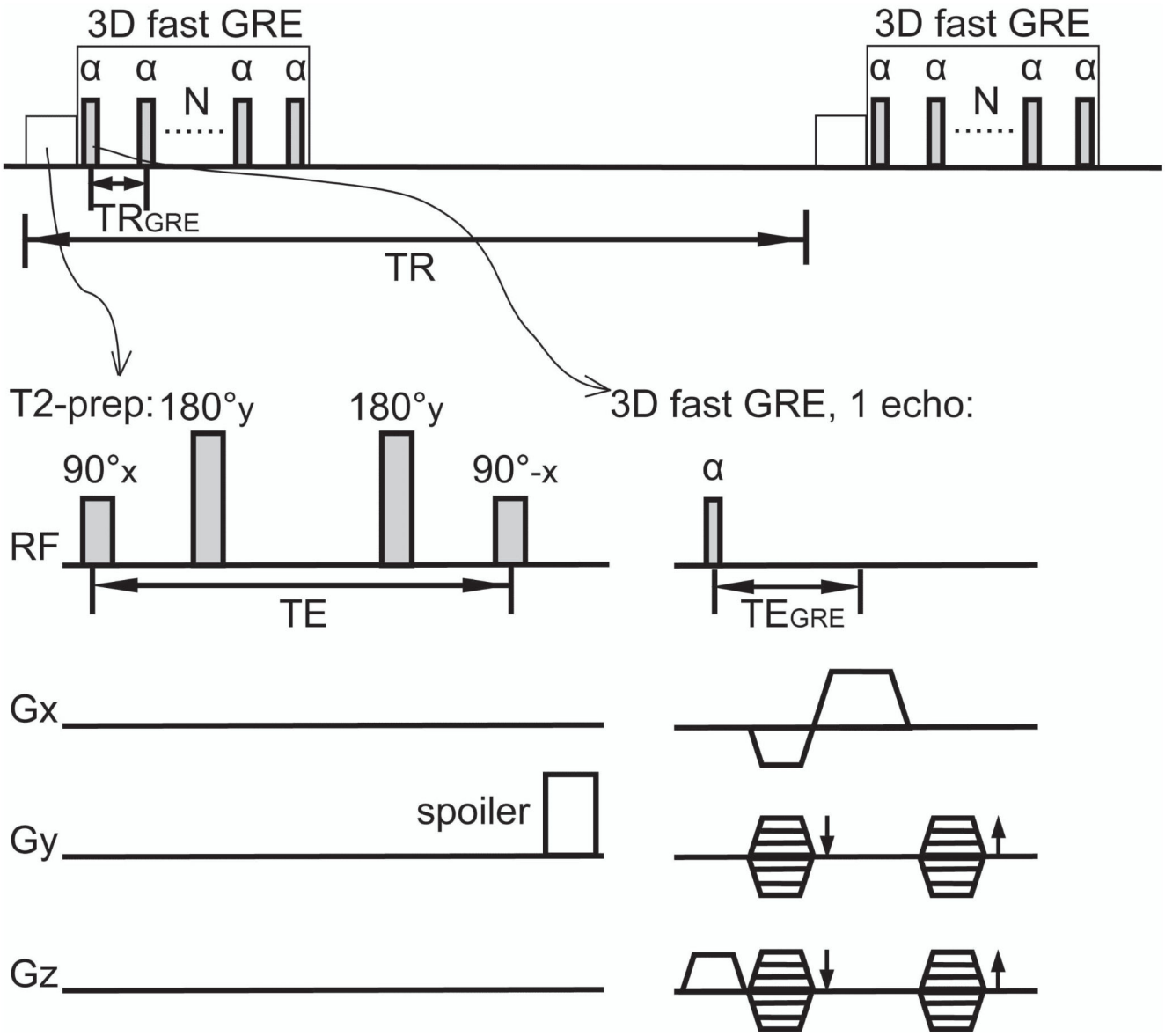

Figure 1.

Pulse sequence of 3D T2prep-GRE. A T2 preparation module (90°x-180°y-180°y-90°-x, spatially non-selective; hyperbolic secant adiabatic pulses were used for 180° pulses) was applied immediately before the readout. Two 180° pulses were used in T2 preparation to compensate phase variations and to suppress inflow effect. A spoiler gradient was played at the end of T2 preparation on the first phase encoding axis that has the lowest gradient duty cycle to dephase any residual transverse magnetization. A single shot 3D fast GRE readout with low-high (centric) phase encoding was used. TR_{GRE}: time period between two consecutive echoes during the fast GRE readout; TE_{GRE}: echo time for one echo in 3D fast GRE; TR: time period between two consecutive 3D fast GRE readout; TE: duration of T2 preparation excluding the spoiler at the end.

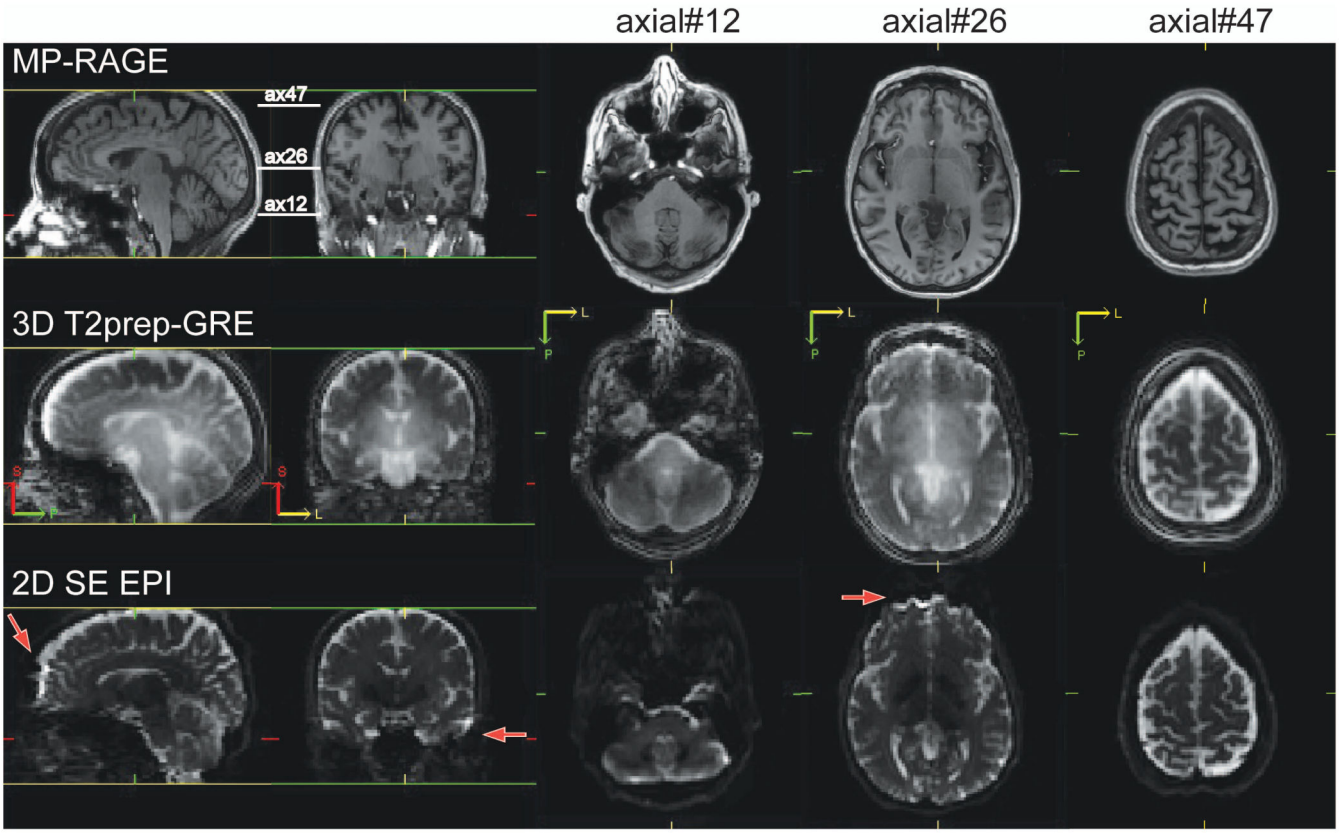

Figure 2.

Comparison of image quality for MPRAGE (anatomical, voxel=1×1×2.5mm^3, 55 slices, reconstructed from the original 1mm isotropic scan), 3D T2prep-GRE fMRI scan (TR=2.3s, 2.5mm isotropic voxel, 55 slices) and 2D multi-slice SE EPI (TR=9s, 2.5mm isotropic voxel, 55 slices, no functional stimulation). Due to SAR limits, 2D SE EPI has to use a TR 4 times longer than 3D T2prep-GRE to acquire the same number of slices covering the whole brain. Sagittal, coronal and 3 axial slices at different locations (slice number 12, 26 and 47) are shown. Geometric distortion is visible in SE EPI images, especially in the frontal and temporal lobes (red arrows). 3D T2prep-GRE images show minimal distortion and dropouts. S: superior; P: posterior; L: left.

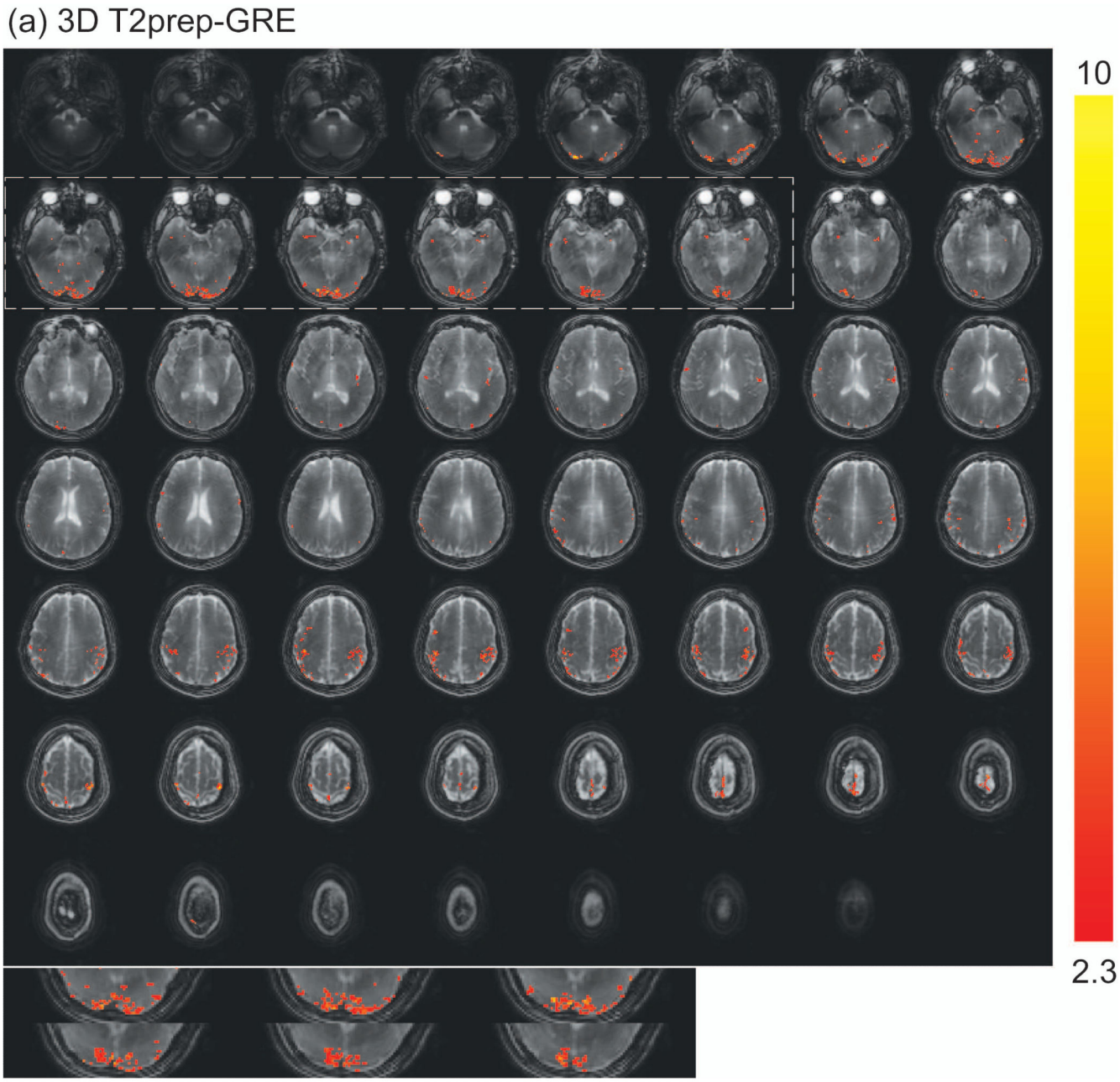

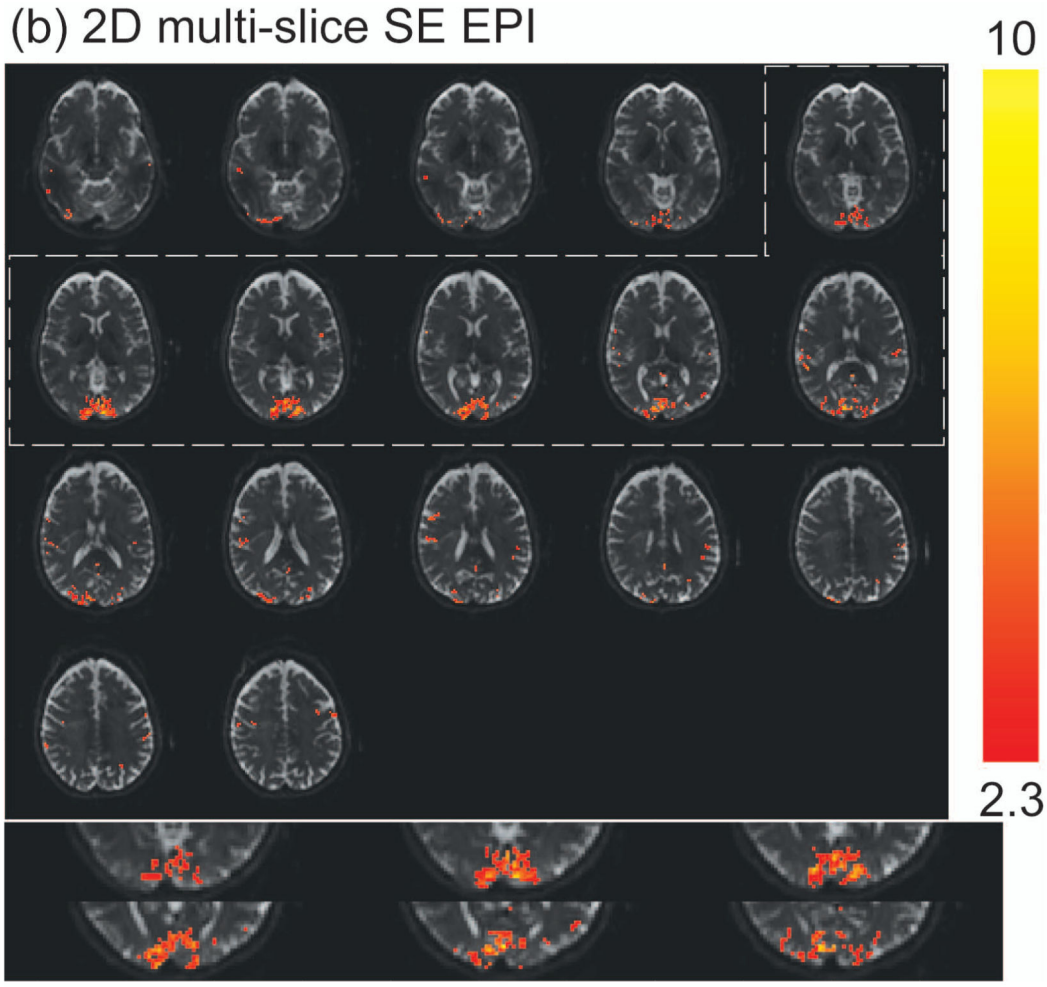

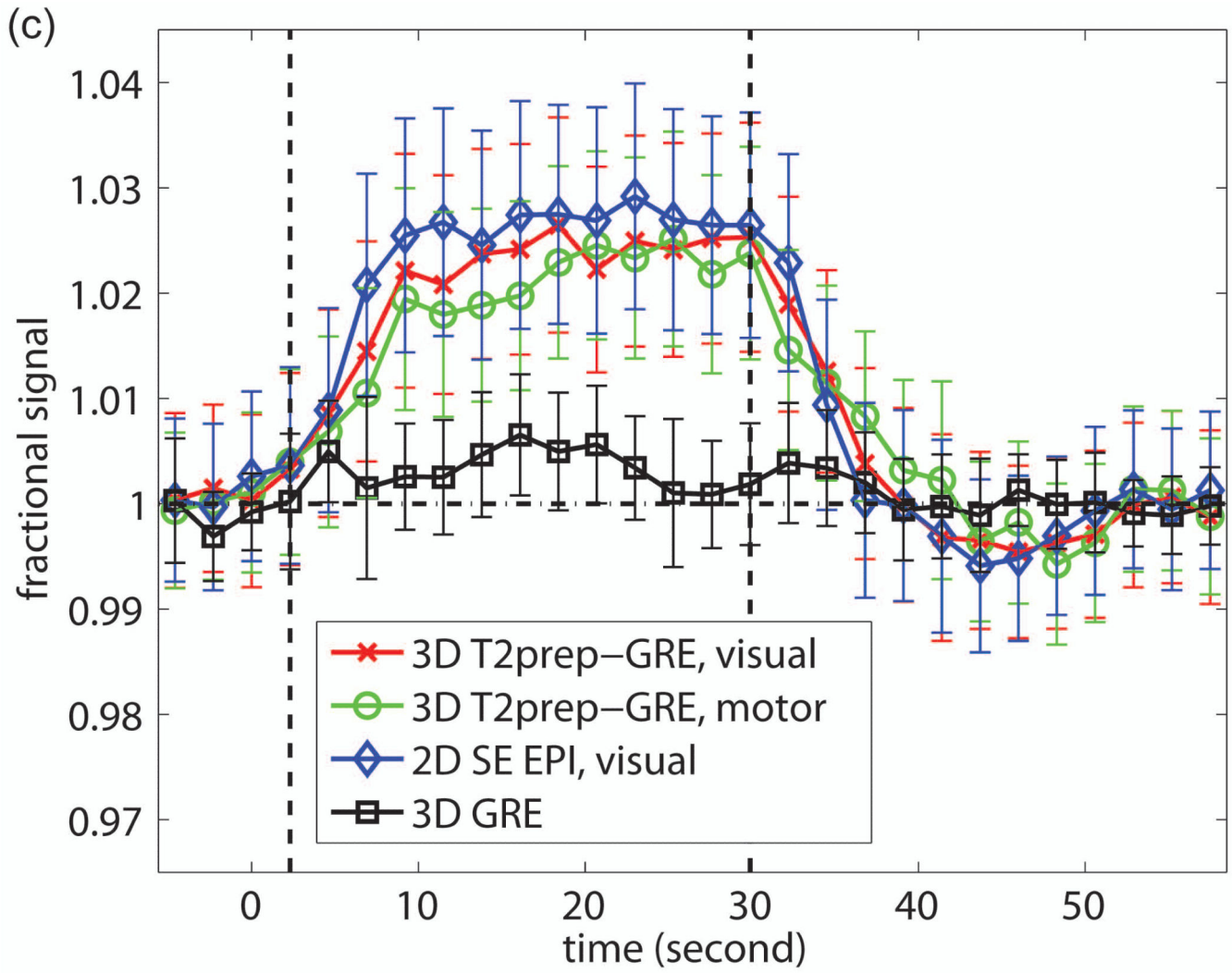

Figure 3.

Representative fMRI results from one subject. **(a)** fMRI activation map with 3D T2prep-GRE (TR=2.3s, 2.5mm isotropic voxel, 55 slices). **(b)** fMRI activation map with 2D multi-slice SE EPI (TR=2.3s, 2.5mm isotropic voxel, 17 slices, angled to cover more cortex and to avoid orbitofrontal cortex). In both (a) and (b), voxels meeting activation criteria are highlighted with their t-scores (scale indicated on the right, threshold=2.3). No spatial smoothing was performed in the analysis. The visual cortex regions in T2prep-GRE and SE EPI images in the dashed boxes are zoomed in and displayed at the bottom of the panels. **(c)** Average time courses from voxels meeting activation criteria in visual (red, x-mark) and motor (green, open circle) cortex with 3D T2prep-GRE, and in visual cortex with 2D SE EPI (blue, diamond). In visual cortex, only common voxels activated in both scans were included. A separate fMRI scan was per-formed using the same 3D fast GRE readout *without* T2 preparation, and the average time course from this scan (black, square) was calculated over voxels activated in the previous 3D T2prep-GRE scan (both visual and motor cortex). Four blocks were averaged to one block. The two vertical dashed lines indicate the start and cessation of stimulus. The error bars represent inter-voxel standard

deviations within subject, which are much larger than the inter-subject standard deviations reported in Table 2.

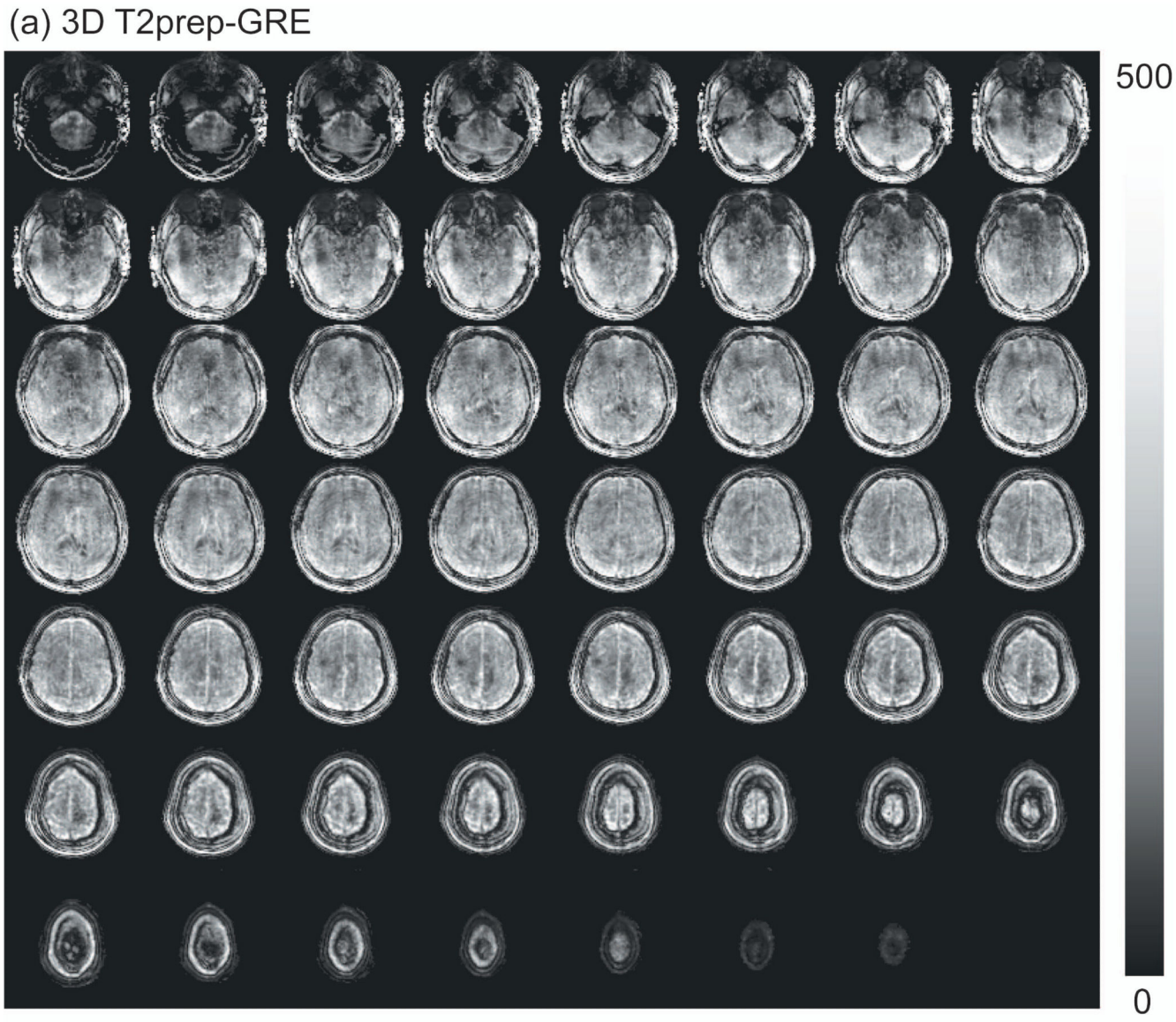

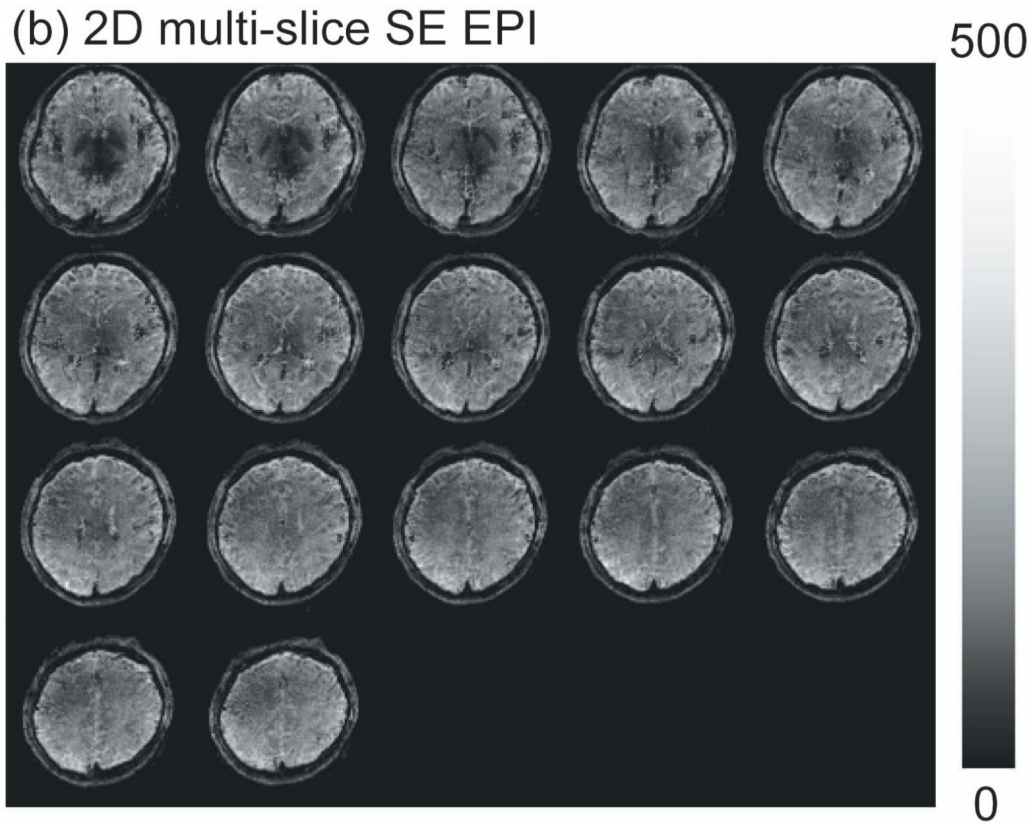

Figure 4.

Representative temporal SNR (tSNR) efficiency maps from one subject. **(a)** 3D T2prep-GRE (TR=2.3s, 2.5mm isotropic voxel, 55 slices); **(b)** 2D SE EPI (TR=2.3s, 2.5mm isotropic voxel, 17 slices, angled to cover more cortex and to avoid orbitofrontal cortex).

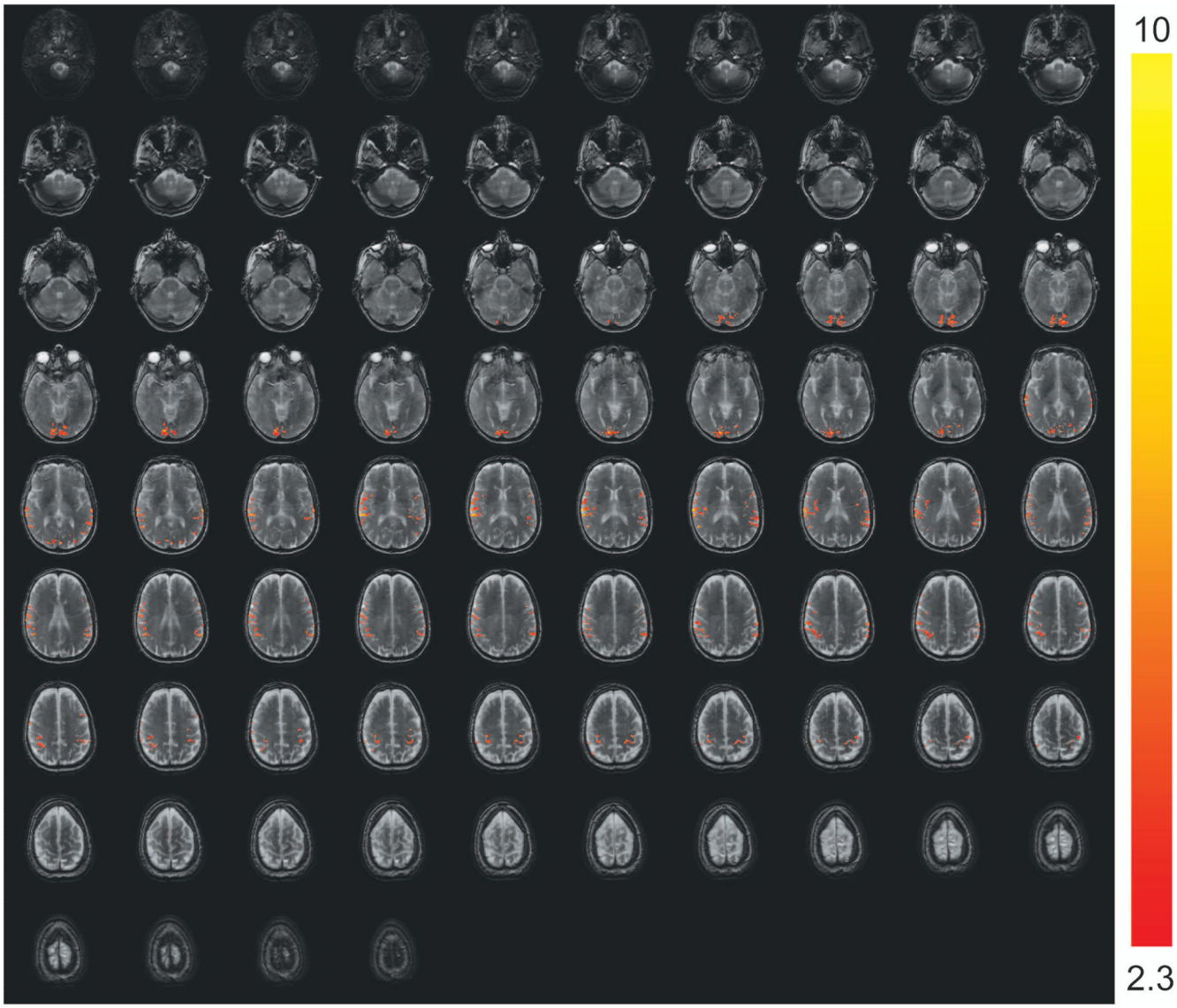

Figure 5.

3D T2prep-GRE fMRI images and activation maps with TR=1860ms, voxel=1.5×1.5×1.6mm^3 and 84 slices from one subject. Voxels meeting activation criteria are highlighted with their t-scores (scale indicated on the right, threshold=2.3).

Table 1

3D T2prep-GRE and 2D multi-slice SE EPI pulse sequences.

	TR(s)	voxel size	slice number	SAR[1]
3D T2prep-GRE (fMRI)	2.3	2.5mm isotropic	55	74%
2D SE EPI (fMRI)	2.3	2.5mm isotropic	17	75%
2D SE EPI (at rest)	9	2.5mm isotropic	55	75%

[1] Specific absorption rate (SAR) shown on the scanner, approximately 2.4W/kg, 74-75% of the maximum SAR approved by FDA.

Table 2

Summary of fMRI results from all subjects.

	shim	cortex	voxel numbers	ΔS/S(%)	tSNR	tSNR efficiency	CNR	CNR efficiency	t-score
Averaged over activated voxels (in visual cortex, voxels activated in all scans) -- without spatial smoothing									
3D T2prep-GRE [a]	volume[c]	visual	340±124	2.5±0.3	58±10	284±30	1.4±0.2	6.5±0.8	3.3±0.1
	volume	motor	304±134	2.3±0.7	56±13	271±43	1.1±0.1	5.2±0.5	3.1±0.1
2D SE EPI [b]	volume	visual	422±181	2.9±0.7	65±16	177±41	1.7±0.2	4.8±0.5	3.6±0.2
	high order[d]	visual	429±176	2.9±0.8	62±18	166±32	1.7±0.2	4.8±0.6	3.6±0.2
Averaged over activated voxels (in visual cortex, voxels activated in all scans) -- with spatial smoothing (5mm FWHM Gaussian kernel)									
3D T2prep-GRE	volume	visual	397±152	2.4±0.3	60±11	292±33	1.4±0.2	6.5±0.8	3.4±0.2
	volume	motor	341±163	2.3±0.6	57±13	275±42	1.1±0.2	5.2±0.6	3.1±0.2
2D SE EPI	volume	visual	498±226	2.7±0.7	64±18	175±47	1.6±0.2	4.7±0.6	3.6±0.2
	high order	visual	485±222	2.7±0.7	66±19	178±52	1.6±0.3	4.7±0.7	3.6±0.2
Averaged over ROIs (GM voxels in primary visual and motor cortex, respectively)									
3D T2prep-GRE	volume	visual	1458±267	0.7±0.1	51±6	247±14	0.4±0.1	1.7±0.4	0.8±0.3
	volume	motor	1046±295	0.6±0.2	48±7	236±20	0.3±0.1	1.3±0.6	0.8±0.4
2D SE EPI	volume	visual	1458±267	0.8±0.5	47±11	128±31	0.4±0.2	0.9±0.4	0.8±0.3
	high order	visual	1458±267	0.8±0.6	45±10	123±30	0.4±0.3	0.9±0.5	0.8±0.3

Mean values ± standard deviations over all subjects (n=5).

Definitions of ΔS/S, tSNR, tSNR efficiency, CNR, and CNR efficiency are described in Methods.

[a] fMRI scan (a).

[b] fMRI scan (b).

[c] Volume shim over a 120×120×50mm^3 (AP×RL×FH) volume centered on the brain was applied in these scans to achieve a reasonably homogeneous field (B0) across the entire brain. A water line width of <60Hz was achieved.

[d] Optimal high order shim in the visual cortex (AP×RL×FH=40×120×50mm^3) using the localized shimming tool developed by Schär et al (59) was applied. A water line width of <60Hz was achieved. Similar results were also obtained with optimal high order shim in the entire brain (data not shown).